Journal of Solid State Chemistry 184 (2011) 1492–1498

Contents lists available at ScienceDirect

Journal of Solid State Chemistry

journal homepage: www.elsevier.com/locate/jssc

Synthesis of carbon-encapsulated iron nanoparticles via solid state reduction of iron oxide nanoparticles

M. Bystrzejewski*

Dept of Chemistry, Warsaw University, Pasteura 1, 02-093 Warsaw, Poland

ARTICLE INFO

Article history:
Received 21 February 2011
Received in revised form
5 April 2011
Accepted 8 April 2011
Available online 21 April 2011

Keywords:
Magnetic nanoparticles
Carbon nanomaterials
Carbothermal solid state reduction

ABSTRACT

The encapsulation of iron nanoparticles in protective carbon cages leads to unique hybrid core–shell nanomaterials. Recent literature reports suggest that such nanocomposites can be obtained in a relatively simple process involving the solid state carbothermal reduction of iron oxide nanoparticles. This approach is very attractive because it does not require advanced equipment and consumes less energy in comparison to widely used plasma methods. The presented more-in-depth study shows that the carbothermal approach is sensitive to temperature and the process yield strongly depends on the morphology and crystallinity of the carbon material used as a reductant.

1. Introduction

Nanocrystallites from magnetic phases are unique nanomaterials because of their size tunable physical and chemical properties [1]. The magnetic nanoparticles with diameters between 1 and 10 nm are superparamagnetic and attain their saturated magnetic response at relatively low external magnetic fields. Larger nanoparticles (10–50 nm) can behave as monodomain objects with giant coercivity fields. Magnetic nanoparticles have found numerous applications that cover data storage [2], catalysis [3], environmental protection [4,5] and various biomedical issues [6–8]. Nevertheless, the utilization of magnetic nanoparticles comprising bare metal phases is not free of significant drawbacks. Such nanomaterials, due to their large surface areas, undergo irreversible oxidation and agglomeration [9]. This in turn changes their properties and worsens magnetic performance. The stability of magnetic nanoparticles can be greatly enhanced when they are protected by external coating layers. Carbon was found to be one of the most superior protecting materials, since it is light, has low magnetic susceptibility and possesses high chemical inertness. Carbon encapsulated nanoparticles were observed for the first time in 1993 during studies on fullerene formation in the carbon arc discharge process [10]. Since that time various synthesis routes of carbon encapsulates have been reported. Nowadays, high temperatures routes including carbon arc discharge [11], flowing thermal plasma jet [12] and flame synthesis [13] are the most selective methods that can be used for fabrication of magnetic carbon nanostructures. The formation of carbon encapsulates via those methods is believed to be driven by a common mechanism. In the early stages, the vapor is saturated with carbon species (C atoms, C_2–C_5 radicals) and metal atoms that will be encapsulated. In the next step the metal-carbon vapor undergoes rapid cooling, which results in condensation of liquid metal nanoparticles with soluble carbon. Further decrease of temperature diminishes the solubility of carbon in the metal, which results in expulsion of carbon coating and solidification of the metal core. The core usually remains in a pure metal phase, however, in some cases the core material forms the carbide phase. In the last 10 years much effort was put to develop a method that can fully supplant the high temperature routes. As for example pyrolysis of metaloorganic compounds was proposed. In fact this method yielded carbon-encapsulated magnetic nanoparticles; however, it required the starting reactants of high complexity (and therefore the high cost) and long reaction times even up to several days [14,15]. Another routes involve two-step processes in which the carbon coatings were deposited onto previously prepared metal nanoparticles with specified diameters [16,17]. The present work is motivated by recent papers demonstrating that carbon-encapsulated iron nanoparticles (CEINs) can be effectively formed by a very simple process—carbothermal reduction (900–1000 °C) of iron oxide nanoparticles by carbon black [18,19]. The both precursors are cheap and environmentally friendly. Moreover the synthesis can be realized in an oven under atmospheric pressure. All this suggests that this route has a huge potential for scaling up. This work is a more-in-depth study of carbothermal process with a special and critical view on actual yields, process selectivity and magnetic characteristics of obtained carbon-encapsulated iron nanoparticles.

---

* Fax: +48 22 822 59 96.
E-mail address: mibys@chem.uw.edu.pl

0022-4596/$ - see front matter © 2011 Elsevier Inc. All rights reserved.
doi:10.1016/j.jssc.2011.04.018

2. Experimental

Alfa-Fe_2O_3 nanoparticles and ultra-fine graphite powder (UG) were purchased from Sigma Aldrich. Carbon black N-330 (CB) was donated by the Research Institute of Rubber Industry (Piastów, Poland). Hollow carbon nanoparticles (CNs) were obtained via combustion synthesis from NaN_3 and C_6Cl_6 as described in detail elsewhere [20]. All experiments were conducted in a horizontal quartz tube (3 cm in diameter and 70 cm in length) reactor placed in a furnace and heated under flowing N_2 (99.999% purity, 400 ml/min at 25 °C). The reactant mixtures contained 70 wt% of Fe_2O_3 nanoparticles and 30 wt% of carbon material (CB, CNs and UG). The as-weighted powders were put in an agate mortar and gently grinded. Then, the mixtures were mixed in a rotary mechanical shaker for 30 min. In the first series the reactant mixtures containing carbon black, hollow carbon nanoparticles and graphite powder were heated in a ceramic boat (7 cm in length and 1.5 cm wide) at 1000 °C for 3 h (Table 1). In the second series one test was performed, in which the Fe_2O_3–CB mixture was annealed at 1200 °C for 3 h. After naturally cooling down to room temperature under flowing N_2 the raw products were collected and weighted (Table 1). Importantly, no solid products were present outside the ceramic boat. The temperature of the reaction zone was precisely controlled by a thermocouple that was coupled with the power supply of the oven.

The raw products were subjected to the purification procedure in order to remove all non-encapsulated metal particles. The procedure included refluxing in boiling 4 M HCl for 24 h, washing with excess of water and ethanol and drying in air at 90 °C for 5 h. The amounts of dry products recovered after acid treatments were monitored and the purification yield was evaluated as the ratio between the recovered mass and the initial mass (Table 1). The raw and purified products were analyzed by scanning (SEM, Leo 1530) and transmission electron microscopy (Libra 120), X-ray powder diffraction (Siemens D500 with a Cu$K\alpha$ radiation), Raman spectroscopy (the spectra were excited using a 532 nm laser) and vibration magnetometry at 25 °C (Lake Shore 668).

3. Results and discussion

3.1. Synthesis of CEINs at 1000 °C

Contrary to the previous literature reports [18,19], three distinct carbon materials were used as reductants, i.e. carbon black, hollow carbon nanoparticles and ultra-fine graphite powder. The used materials differ distinctly in morphology and crystallinity, and those factors may influence the encapsulation of iron nanoparticles. CB and CNs are composed of uniform nanoparticles with diameters below 100 nm (Fig. S1). A dominant fraction of the CN material is comprised of hollow nanoparticles with empty cores [20], whilst CB contains solid particles only. The external diameter and size of the core in CNs are comparable to the geometrical parameters of CEINs obtained via plasma methods and flame synthesis [12,13]. Due to this morphological similarity between CNs and CEINs, the hollow carbon nanoparticles may have greater potential in encapsulation of Fe nanoparticles in comparison to carbon black. Graphite powder contains typical flake crystallites with size between 1 and 10 μm. The studied carbon materials have distinct crystallinity, which can be derived from the position of the (002) reflection (Fig. S2). The graphitization degree of the studied samples changes in the following order: UG > CB > CNs. The crystallinity may also have an impact on the reaction rate between the iron oxide and the solid carbon. The carbon material with lower graphitization degree (i.e. being more amorphous) should react faster, because of lower lattice energies. In fact, it was demonstrated that the activation energy for high-temperature reduction of iron oxides by poorly crystallized charcoal was lower in comparison to graphite [21].

Table 1
Operational parameters.

Test	Process temperature (°C)	Type of carbon material	Initial mass of reagents (g)	Mass of products (g)	Purification yield (%)
1	1000	Carbon black	2.000	1.342	37.5
2		Carbon nanoparticles	2.000	1.300	16.7
3		Ultra-fine graphite powder	2.000	1.423	24.5
4	1200	Carbon black	2.000	1.134	28.0

The reaction between Fe_2O_3 and solid carbon at high temperatures occurs by the following scheme: $Fe_2O_3+3C\rightarrow 2Fe+3CO$. The process is thermodynamically and kinetically favored at temperatures above 800 °C. It has been shown that the reduction of Fe_2O_3 to the elemental Fe can run through two parallel channels, which are pronounced by the presence of transition phases: FeO and Fe_3O_4 [22]. Fig. 1 shows XRD patterns of raw and purified products from experiments conducted at 1000 °C. Three Fe-containing crystallites were found to be present in raw products: bcc Fe, Fe_3O_4 and non-stoichiometric Fe_xO ($x=0.96$). The x value was evaluated from the lattice constant, which was calculated from the position of the (111) reflection [23]. There were no qualitative differences in phase composition for raw products obtained from three various carbon materials. In each case, the reflection for the bcc Fe is the strongest, which shows that the content of this phase significantly exceeds the fraction of still present iron oxides. This findings are in disagreement with previous reports [18,19], showing that the annealing temperature of 1000 °C and reaction time 2 h are sufficient to totally reduce all iron oxides to the pure metal phase. The presence of iron oxides is also reflected by the mass of collected products. Assuming the reaction scheme shown above, the mass of products should be 1.265 g (see Section S2 in Supplementary Data). In each case, the mass of products is higher than this value (Table 1), which can be explained by the presence of the unreduced iron oxide.

The purified products have different diffraction patterns in comparison to the raw products. The intensity of Fe reflection decreases substantially and the $Fe_{0.96}O$ and Fe_3O_4 phases prevail in samples from Tests 1 and 2. The XRD pattern of the purified product from Test 3 has a strong feature from graphite, whilst reflections from bcc Fe and iron oxides are very weak and have comparable intensities. The purification leaches all Fe-based particles that are not protected and undergo dissolution in contact with acid. This is also depicted in values of the purification yield, which show how much of the solid product is recovered after acid treatment (Table 1). The yields for Tests 1 and 3 are positively deviated from the theoretical value of 22.5% (this number refers to the situation, in which all Fe particles are leached in acid, see Section S3). In the case of Test 2, the yield is lower than 22.5%, which can be explained by the fact that a fraction of CNs was gasified during the reaction. As shown earlier the CN material has the lowest graphitization degree and therefore can react at high temperature with traces of water vapor and oxygen that are always present as contaminants in the buffer gas. All above findings point that the moderate graphitization degree (as for the case of carbon black) is the most optimal for obtaining the best purification yield.

The raw products (Fig. 2) have distinct morphology in comparison to the starting reagents (Fig. S1). The samples synthesized from carbon black and graphite contain large non-uniform "glassy" objects, which can be ascribed to the reduced Fe. The

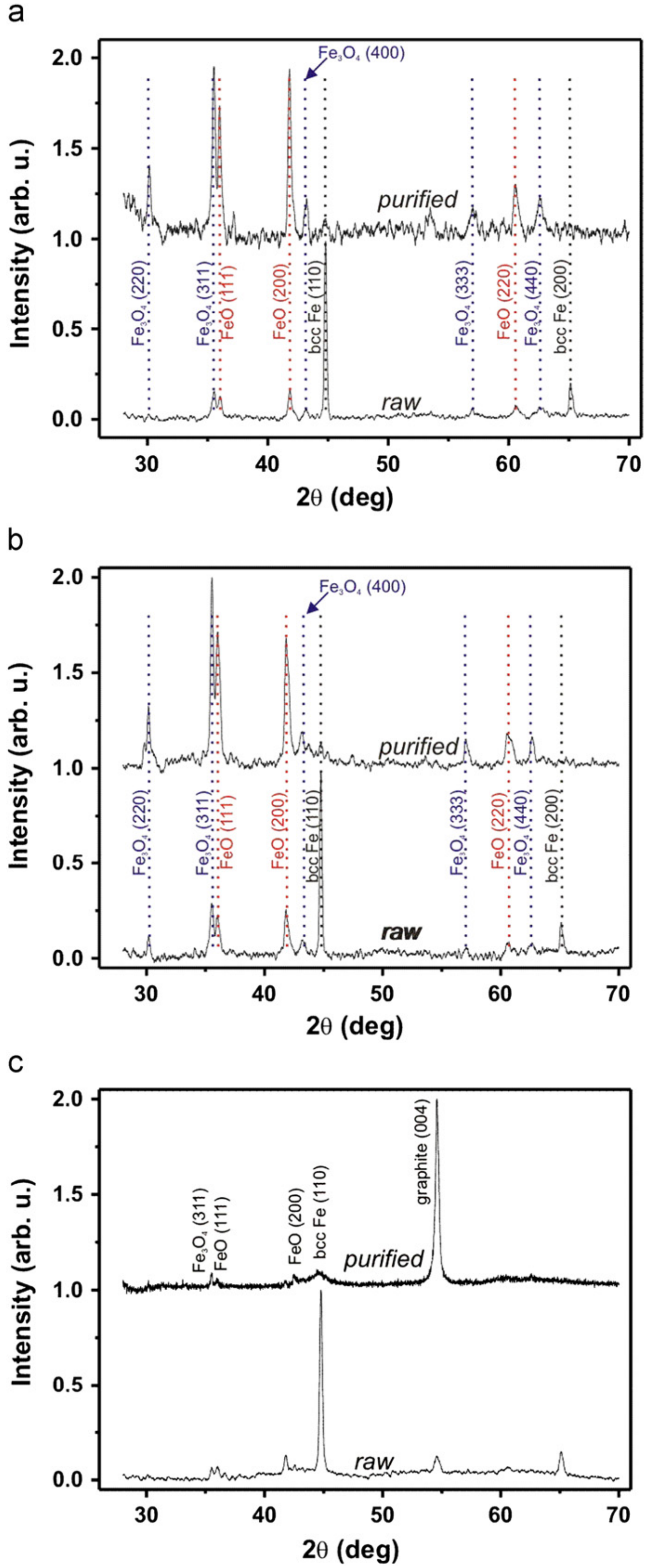

Fig. 1. X-ray diffraction patterns of raw and purified products from Test 1 (a), Test 2 (b) and Test 3 (c).

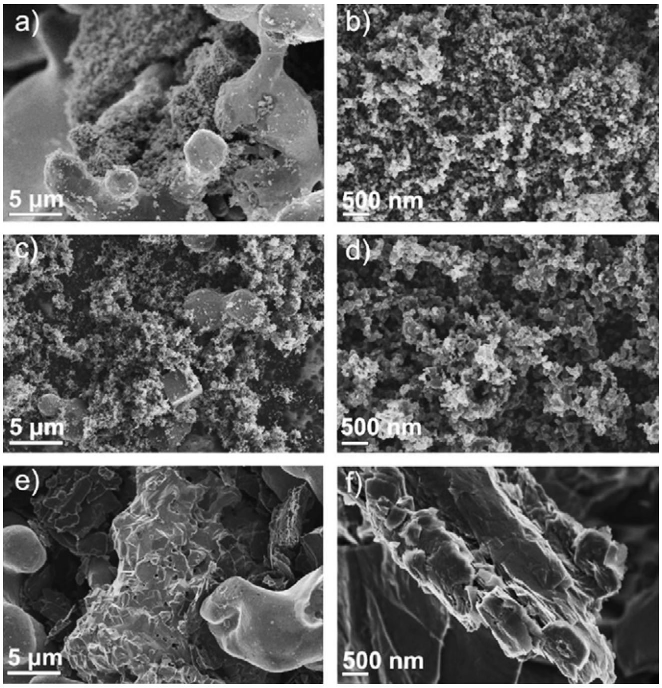

Fig. 2. SEM images of raw (left column) and purified (right column) products from Test 1 (a and b), Test 2 (c and d) and Test 3 (e and f).

use of hollow carbon nanoparticles results in cubic and spherical Fe particles (2–10 μm). In each case the Fe particles are mixed with the remaining carbon material, which has not been used during the process. The acid treatment removes the micro-size Fe particles and the morphology of the purified samples resembles the microscopic features of the starting CB, CN and UG materials. This observation also agrees with the XRD data, which point to large reduction of amounts of Fe crystallites. Finally, it shows that the carbothermal reduction of iron oxide nanoparticles primarily results in large Fe particles that are easily leachable by acids. The previous literature investigations did not consider the overall morphology studies and the reader might have an impression that all Fe crystallites obtained from iron oxide nanoparticles were in a form of CEINs [18,19].

TEM studies were conducted to visualize the morphology of the Fe-containing crystallites appearing in XRD patterns of the purified products. The product obtained from carbon black is primarily composed of CB particles with small amounts of well crystallized CEINs (Fig. 3a). The CEINs have diameters between 50 and 100 nm, and the thickness of carbon coating is ca. 10 nm. Occasionally, the sample contains solid metal (or metal oxide) crystallites of non-uniform shape, which are covered by surrounding carbon black particles (Fig. 3b). This type of structures cannot be regarded as carbon encapsulates. Nevertheless, the metal crystallites covered by adjacent CB particles were sufficiently protected and did not undergo the acid leaching. The use of hollow carbon nanoparticles as a reductant yields the product in which the carbon-encapsulated iron nanoparticles were not found. Similar to Test 1, the sample contains metal particles covered by the particles of the starting material (Fig. 3c and d). Detailed TEM studies of product synthesized from graphite revealed neither CEINs nor metal particles covered by graphite particles. The lack of these structure is in an apparent disagreement with the XRD data, which show that metal crystallites *are* present. However, the XRD peaks have low intensity (in comparison to the intense (004) reflection for graphite) and this makes the observation of metal crystallites in TEM practically impossible.

The performed structural and morphological studies show that the carbothermal reduction of iron oxide nanoparticles yields primarily Fe microparticles with some amounts of carbon encapsulates and heterogeneous structures having a form of metal/metal oxide core—carbon coating. However, those observations provide qualitative information only. Basic magnetic inspection

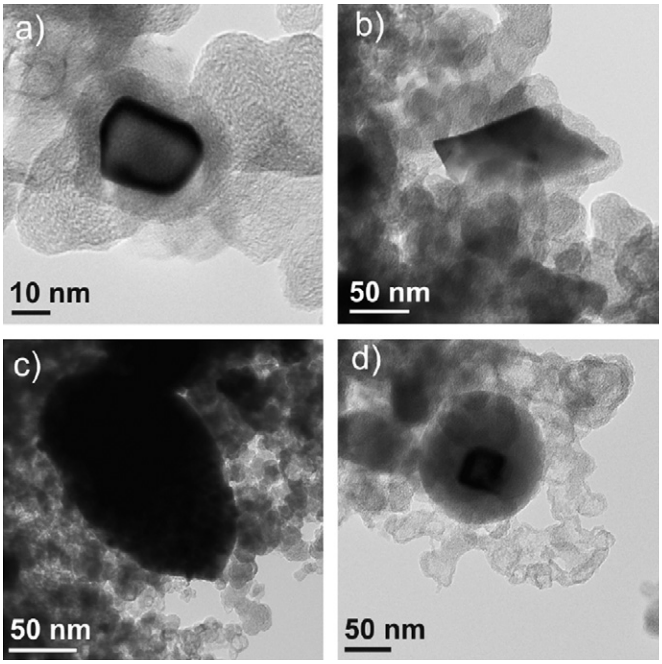

Fig. 3. TEM images of purified products from Test 1 (a and b) and Test 2 (c and d).

Table 2
Qualitative phase composition and saturation magnetization for raw and purified products.

Test	Phases identified		M_s (emu/g)	
	Raw product	Purified product	Raw product	Purified product
1	C, bcc Fe, $Fe_{0.96}O$, Fe_3O_4	C, $Fe_{0.96}O$, Fe_3O_4, bcc Fe	125	20
2		C, $Fe_{0.96}O$, Fe_3O_4, bcc Fe	138	5
3		C, $Fe_{0.96}O$, Fe_3O_4, bcc Fe	132	1
4	C, bcc Fe, fcc Fe-C, Fe_3O_4	C, bcc Fe, fcc Fe-C	62	6

(e.g. magnetization measurements) may give half-quantitative composition of the samples, since the raw and purified products are comprised of materials that are ferromagnetic at room temperature and their magnetic susceptibilities are known. The hysteresis loops for raw products are shown in Fig. S3. The saturation magnetization (M_s) of the starting Fe_2O_3 material agrees with other literature data [13]. The M_s values for raw products are between 125 and 132 emu/g (Table 2) and they are comparable to the magnetization reported by Tokoro et al. (101 emu/g). The obtained M_s values are lower in comparison to the estimated theoretical $M_s = 174$ emu/g (see Supplementary Data). This is a consequence of the fact that a fraction of Fe in raw products is in the form of oxides, which have weaker magnetic moment. The purified products have very distinct magnetic characteristics (Fig. S4). The saturation magnetizations (Table 2) are one order of magnitude lower in comparison to the raw samples and to the values reported by Tokoro et al. [18,19]. This points to the low content of magnetic nanostructures in purified products and is in agreement with microscopic observations. Moreover, it can be concluded that carbon black is the most appropriate reductant in the carbothermal process, because its use results in the product with the best magnetic characteristics.

3.2. Synthesis of CEINs at 1200 °C

The experiments conducted at 1000 °C resulted in small amounts of carbon-encapsulated iron nanoparticles. The obtained low process yield and non-specific selectivity may be related to temperature. According to the Fe–C diagram at 1000 °C all phases that were visualized on the XRD patterns exist in a solid state. Generally, the kinetics of the solid state reactions is mainly limited by diffusion processes. This limitation may be omitted, when at least one of the reactants will be in the liquid phase. According to the Fe–C diagram there is an eutectic point (1148 °C) for the Fe content of 4.3 wt%. To verify this idea an experiment was conducted at 1200 °C, i.e. under those conditions the as-reduced iron will be in a liquid state. The experiment was carried out with carbon black only, because this material yielded carbon-encapsulated iron nanoparticles at lower temperatures. The raw product contains bcc Fe, Fe_3O_4 and fcc Fe-C crystallites (Fig. 4). The fcc Fe–C phase is a solid solution of C in fcc Fe. The composition of the raw product is different when compared to Test 1, because of the lack of FeO. The presence of Fe_3O_4 proves that, despite the higher temperature, a fraction of the starting iron oxide has still not been reduced to metallic Fe. The fcc Fe–C

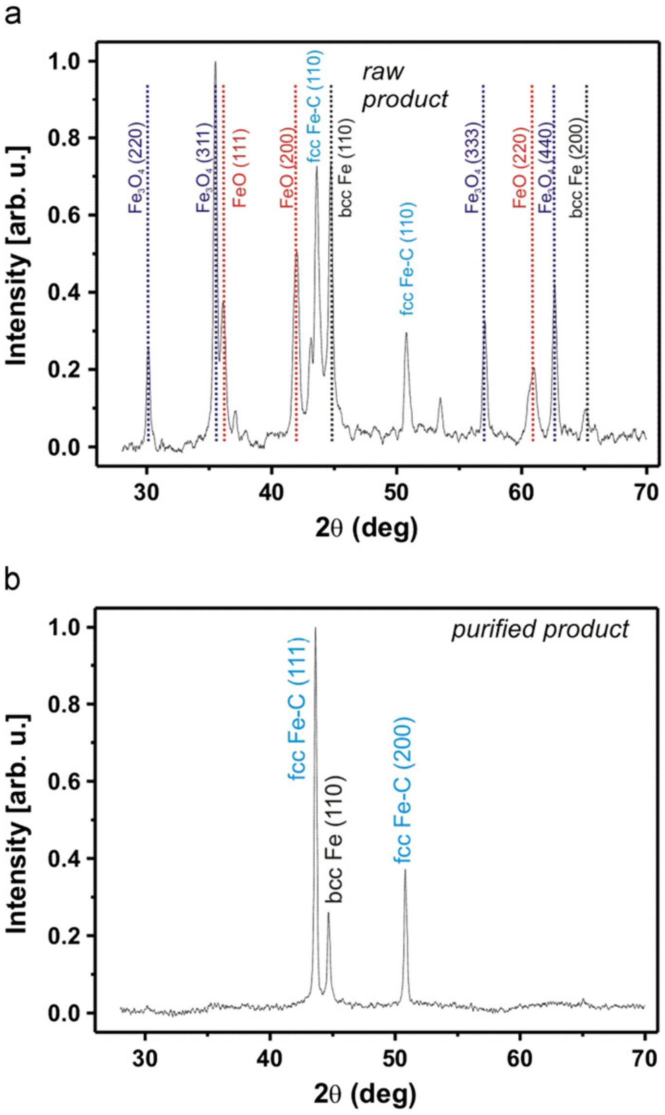

Fig. 4. X-ray diffraction patterns of raw (a) and purified (b) products from Test 4.

crystallites are not thermodynamically stable at room temperature, nevertheless this phase is frequently found in CEINs synthesized via various techniques [24]. The mass of collected raw product is lower than the theoretical value 1.265 g (Table 1). Unambiguously, this reduction of the mass is related to gasification of the fraction of carbon black particles. Despite the lower mass of the raw product, the purification yield is higher than the critical yield (22.5%). This observation clearly demonstrates that a part of metallic particles has not been leached by the acid and might be encapsulated in carbon. In fact, the purified sample contains XRD signatures that are ascribed to the fcc Fe–C and bcc Fe crystallites. Moreover, the relative intensity of reflections points to the higher content of fcc phase. Importantly, no reflections arising from iron oxides were found. This shows that the higher process temperature increases the process selectivity.

The morphology of the raw product is generally similar when compared to the samples obtained at 1000 °C. The regular Fe microparticles are randomly distributed in a carbon black matrix in the raw product (Fig. 5a). After purification the microparticles are removed and the sample consists of spherical nanoparticles with diameters ranging between 50 and 200 nm (Fig. 5b). TEM inspection reveals that the purified product is comprised of CB particles and carbon encapsulates (Fig. 6a). The encapsulates have spherical and ovals shapes, and their diameters are between 100 and 200 nm. Some amounts of micro-sized hollow carbon structures were also found (Fig. 6b). The empty core and the discontinuity in the side wall suggest that this particle was the large Fe-filled capsule (acid treatment resulted in complete leaching of the metallic core). In fact, its size agrees with the diameters of microparticles visualized in SEM image. Some CEINs have interesting defects in the coatings, which are characterized by the internal cavity (Fig. 6c and d). Despite this fault, the carbon coating survives the acid treatment and fully protects the encapsulated Fe core. It is worth to notice that TEM observations did not reveal the presence of metal (or metal oxides) crystallites wrapped in carbon particles (these structures were primarily found in samples synthesized at lower temperature). This strongly highlights that the temperature, as an easily controlled parameter, drives the process selectivity.

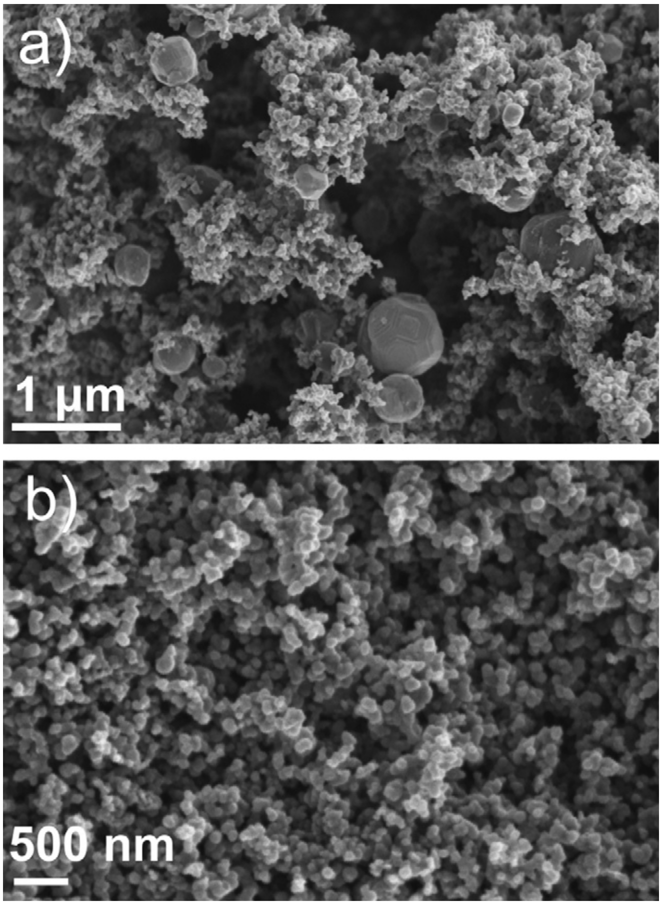

Fig. 5. SEM images of raw (a) and purified (b) products from Test 4.

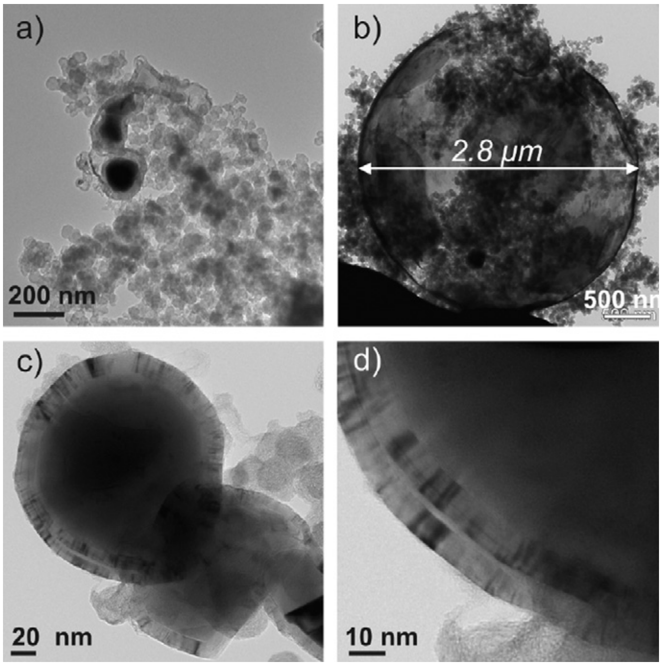

Fig. 6. TEM images of purified products from Test 4.

The magnetic characteristics of raw and purified products from Test 4 (Table 2) are distinct to the samples from Tests 1 to 3 (hysteresis loops are shown in Fig. S5). The saturation magnetization of the raw product is ca. 2 times lower in comparison to the products obtained at 1000 °C. This is an implication of different phase composition—higher temperature favors formation of fcc Fe–C, which is paramagnetic at room temperature and practically has no contribution to the magnetic moment. The same observation refers to the purified product, which has the M_s of 6 emu/g only. This value can be used to evaluate the bcc Fe content only, whilst the total Fe content should be estimated by the method that will be sensitive to the presence of the bcc and fcc phases. The direct comparison of the experimental M_s and the M_s for the bulk bcc Fe (224 emu/g) points to the bcc Fe content of 2.7 wt%. The total Fe content was evaluated by a thermogravimetric method. The purified sample (100 mg) was burned in air at 900 °C, and the as-formed residue was weighted (the average mass from three repetitions was 10.3 ± 0.5 mg). The XRD study showed that this residue contains Fe_2O_3 crystallites only. Simple stoichiometric calculations allowed to evaluate the total Fe content, which was found to be 7.2 ± 0.4 wt%. This value referred to the Fe content in the initial mixture (70 wt% Fe_2O_3 is an equivalent of 49 wt% Fe) informs about the amount of Fe which has been encapsulated. Thus, the so-called encapsulation rate is found to be ca. 15%. Please note that this parameter can be also evaluated for the samples synthesized at 1000 °C. However, the interpretation and other comparisons will be ambiguous due to the diversity of phase composition (metallic Fe, iron oxides) and miscellaneous morphology (CEINs vs. particles wrapped in carbon particles).

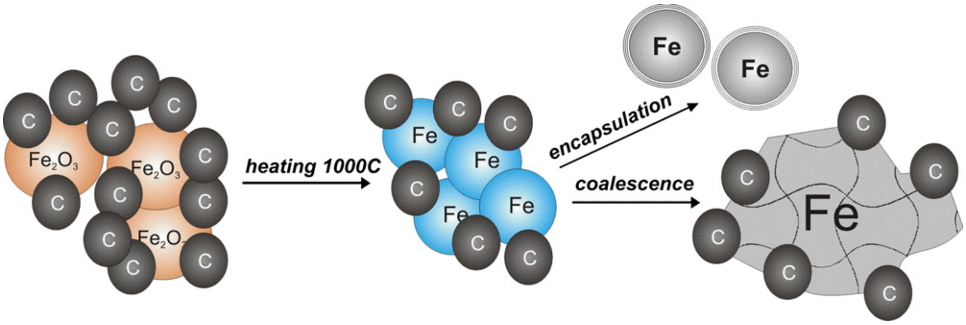

Fig. 7. Three reaction pathways in carbothermal reduction of iron oxide nanoparticles.

3.3. *Formation mechanism of CEINs*

The results presented above clearly demonstrate that the formation of CEINs is affected by the process temperature and the structure of carbon reductant. The details of structural and morphological analyses point to at least three parallel reaction pathways (Fig. 7). The first of them is directly related with the reduction of iron oxide by carbon. This is the most important step, in which the metallic Fe nanoparticles are produced. Next, the as-reduced Fe nanoparticles can undergo two parallel pathways: (i) coalescence into microparticles and (ii) encapsulation in carbon. The mechanism of encapsulation at the applied experimental conditions (temperatures 1000–1200 °C) is obviously different than in the gas phase growth of CEINs. In the latter case, high temperature enables formation of the Fe–C gas, which further undergoes quenching, condensation, nucleation and solidification to CEINs [25]. At temperatures lower than the vaporization point of Fe an another mechanism must be considered. It is known that transition metals are the elements that have superior graphitization properties [26]. Annealing of poorly crystallized solid carbon with, e.g. Fe crystallites, may result in re-structuring of the carbon phase to the highly graphitized material. If the Fe crystallite is small then it can graphitize the surrounding carbon to obtain the encapsulate with a tight carbon coating. The graphitization and the encapsulation likely occurs within the frames of the liquid–solid mechanism. First, the carbon (from carbon particles surrounding the Fe particle) dissolves in a hot metal particle. Then it precipitates in the form of graphitized surface layer (the precipitation can be triggered by temperature gradient). In fact, it has been recently demonstrated by *in situ* TEM studies that heating of Fe nanoparticles supported onto amorphous carbon led to graphitization of the carbon phase and encapsulation of Fe nanoparticles [27]. The results presented above show that CEINs can be formed, but the micro-size Fe particles prevail in the products from all tests. This observation suggests that the majority of the as-reduced Fe nanoparticles coalesce into larger objects and only some of them can be encapsulated. In other words, the rate of coalescence exceeds the rate of encapsulation. This undesired coalescence process would be substantially reduced by increasing the content of carbon in the reactant mixture. In such case, the as-reduced Fe particles would be distributed more homogenously in the carbon matrix with the lower probability of the surface contact. The verification of that hypothesis is underway.

4. Conclusions

The carbothermal solid state reduction of iron oxide nanoparticles was studied. According to the previous literature reports this facile process has a big potential for fabrication of carbon-encapsulated iron nanoparticles. The unquestioned advantages stem from low cost starting reagents and simple construction of the reactor. The aim of this work was to perform a more-in-depth study of this process. Three various carbon materials were tested as reductants: carbon black, hollow carbon nanoparticles and ultra-fine graphite powder. The process performed at 1000 °C was non-selective and yielded micro- and nanoparticles comprising of Fe and partially reduced oxides ($Fe_{0.96}O$ and Fe_3O_4). Carbon-encapsulated iron nanoparticles were found in a very few amounts in sample obtained from carbon black only. The purified products obtained from other carbon reductants contained iron oxide nanoparticles wrapped in carbon matrix. The increase of temperature to 1200 °C significantly improved the selectivity. The purified product comprised well crystallized spherical carbon-encapsulated iron nanoparticles with diameters between 100 and 200 nm. On the basis of the magnetic and thermogravimetric measurements it was found that 15% of the starting amount of Fe has been encapsulated in carbon. The results obtained in this study shows that the carbochemical solid state reduction of iron oxide nanoparticles is an interesting method for fabrication of iron-encapsulated iron nanoparticles. The moderately high encapsulation yield at 1200 °C make this synthesis route to be competitive with gas phase fabrication techniques of CEINs.

Acknowledgments

This work was supported by the Ministry of Science and Education through the Department of Chemistry, Warsaw University, under Grant N N204 132137. The author thanks H. Lange, A. Huczko and M. Soszyński for comments and remarks.

Appendix A. Supplementary Data

Supplementary data associated with this article can be found in the online version at doi:10.1016/j.jssc.2011.04.018.

References

[1] S.P. Gubin, Magnetic nanoparticles, Weinheim, 2009.
[2] G. Reiss, A. Hutten., Nat. Mater. 10 (2005) 725–726.
[3] U. Laska, C.G. Frost, G.J. Price, P.K. Plucinski, J. Catal. 268 (2009) 318–328.
[4] M. Bystrzejewski, K. Pyrzyńska, A. Huczko, H. Lange, Carbon 47 (2009) 1201–1204.
[5] S.V. Kolotilov, O. Shvets, O. Cador, N. Kasian, V.G. Pavlov, L. Ouahab, et al., J. Solid State Chem 179 (2006) 2426–2432.
[6] I.K. Herrmann, R.N. Grass, W.J. Stark, Nanomedicine 4 (2009) 787–798.
[7] A.A. El-Gendy, E.M.M. Ibrahim, V.O. Khavrus, Y. Krupskaya, S. Hampel, A. Leonhardt, et al., Carbon 47 (2009) 2821–2828.
[8] M. Bystrzejewski, M.H. Rummeli, Pol. J. Chem 81 (2007) 1219–1255.

[9] E.E. Carpenter, S. Calvin, R.M. Stroud, V.G. Harris, Chem. Mater. 15 (2003) 3245–3246.
[10] R.S. Ruoff, D.C. Lorents, B. Chan, R. Malhotra, S. Subramoney, Science 259 (1993) 346–347.
[11] J. Borysiuk, A. Grabias, J. Szczytko, M. Bystrzejewski, A. Twardowski, H. Lange, Carbon 46 (2008) 1693–1701.
[12] M. Bystrzejewski, Z. Karoly, J. Szepvolgyi, W. Kaszuwara, A. Huczko, H. Lange, Carbon 47 (2009) 2040–2048.
[13] I.K. Herrmann, R.N. Grass, D. Mazunin, W.J. Stark, Chem. Mater 21 (2009) 3275–3281.
[14] N.S. Kopelev, V. Chechersky, A. Nath, Z.L. Wang, E. Kuzmann, B. Zhang, G.H. Via, Chem. Mater. 7 (1995) 1419–1421.
[15] S.C. Tsang, J.Q. Qiu, P.J.F. Harris, Q.J. Fu, N. Zhang, Chem. Phys. Lett. 322 (2000) 553–560.
[16] C.N. He, X.W. Du, J. Ding, C.S. Shi, J.J. Li, N.Q. Zhao, et al., Carbon 44 (2006) 2330–2333.
[17] U. Narkiewicz, M. Podsiadły, Appl. Surf. Sci. 256 (2010) S249–S253.
[18] H. Tokoro, S. Fujii, T. Oku, Diamond Rel. Mater 13 (2004) 1270–1273.
[19] H. Tokoro, S. Fujii, T. Oku, J. Magn. Magn. Mater. 290–291 (2005) 141–144.
[20] M. Bystrzejewski, M.H. Rümmeli, T. Gemming, H. Lange, A. Huczko, New Carbon Mater. 25 (2010) 1–8.
[21] D.M. dos Santos, M.B. Mourao, Scand. J. Metall. 33 (2004) 229–235.
[22] K. Mondal, H. Lorethova, E. Hippo, T. Wiltowski, S.B. Lalvani, Fuel Proc. Technol 86 (2004) 33–47.
[23] C.A. McCammon, L.G. Liu, Phys. Chem. Miner. 10 (1984) 106–113.
[24] M. Bystrzejewski, A. Grabias, J. Borysiuk, A. Huczko, H. Lange, J. Appl. Phys. 104 (54307) (2008) 1–8.
[25] B.R. Elliott, J.J. Host, V.P. Dravid, M.H. Teng, J.J. Hwang, J. Mater. Res. 12 (1997) 3328–3344.
[26] A. Oya, H. Marsh, J. Mater. Sci. 17 (1982) 309–322.
[27] R. Anton, Carbon 47 (2009) 856–865.